Materials Today Communications xxx (xxxx) 104950

Contents lists available at ScienceDirect

Materials Today Communications

journal homepage: www.elsevier.com/locate/mtcomm

Facile fabrication of novel europium doped strontium yttrate ($SrY_2O_4:Eu^{3+}$) electrospun nanofibers for flexible display applications

Mahelaqua A. Haque [a], Mahejabeen Azizul Haque [b], Subhash B. Kondawar [a, *]

[a] Department of Physics, Rashtrasant Tukadoji Maharaj Nagpur University, Nagpur 440033, India
[b] Department of Chemistry, Bajaj College of Science, Wardha 442001, India

ARTICLE INFO

Keywords:
Electrospinning
$SrY_2O_4:Eu^{3+}$ nanofibers
Photoluminescence
Flexible display

ABSTRACT

Novel europium doped strontium yttrate ($SrY_2O_4:Eu^{3+}$) nanofibers have been firstly synthesized by electrospinning. $SrY_2O_4:Eu^{3+}$ nanofibers have been systematically examined at different calcination temperatures. The TGA study reveals the thermal behaviour of $SrY_2O_4:Eu^{3+}$ nanofibers which stabilises at 900°C. $SrY_2O_4:Eu^{3+}$ nanofibers have an average diameter of 328 nm before calcination and 162 nm post calcination. X-ray diffraction (XRD) spectra of $SrY_2O_4:Eu^{3+}$ nanofibers revealed the orthorhombic phase with *Pnam* space group. The ionic radii and charge compensation have significant effect on the XRD and photoluminescence (PL) spectra of $SrY_2O_4:Eu^{3+}$ nanofibers. PL spectra was observed under 395 nm excitation and a strong emission line spotted at 612 nm is attributed to characteristic electric dipole transition $^5D_0 \rightarrow {}^7F_2$ of Eu^{3+} ion. Effect of dopant concentration on PL of host $SrY_2O_4:Eu^{3+}$ nanofibers have also been explored. SrY_2O_4 nanofibers doped with 10 mol % of Eu^{3+} ions exhibit optimum emission intensity while concentration quenching is observed for higher dopant concentration. The $SrY_2O_4:Eu^{3+}$ nanofibers show affirmative agreement with $SrY_2O_4:Eu^{3+}$ bulk counterpart. The CIE coordinates for $SrY_2O_4:Eu^{3+}$ nanofibers appear in red region with good colour purity. $SrY_2O_4:Eu^{3+}$ nanofibers possess inherent luminescence property which makes it potential candidate for flexible display applications.

1. Introduction

The rosy dream of push button life and automation has eased the life of human beings. However, the emerging trend of research and innovation has facilitated man to explore new horizons of science and technology. One such dimension to this new horizon is smart materials. Any material that can sense or react to external stimuli can be categorised as smart material. The stimuli can be in varied forms such as environmental, physical, chemical, biological, thermal, optical, electrical, etc [1–4]. Luminescent nanomaterials have garnered great research interest ever since miniaturisation of display devices [5–7]. Smart luminescent materials constitute diverse applications as polymeric optical fibers, light emitting diodes (LEDs), display devices, self-emitting devices, light sensors, and many more [8–12]. A major limitation to smart materials for flexible electronic devices is the flexibility and endurance of the material and electronics incorporated into the device, without debasement of its performance [13–18]. Nanotechnology effortlessly helps in overcoming this impediment. Numerous nanomaterials have been reported to be useful as smart materials [19–22]. Among these, nanomaterials have largely been explored in the form of thin films or nanoparticles sprinkled onto the substrate, yet they cease to function by virtue of lack of flexibility and weathering of the nanoparticles off the substrate [23–28]. Nanofibers (NFs) are one such type of nanomaterial which could easily fill this gap owing to its flexibility and majorly because they exhibit intrinsic property within the fiber itself [29–31]. Various physical and chemical methods are available for the fabrication of NFs, but electrospinning is a superficial way for preparing NFs. Electrospinning method has several controllable parameters which makes the synthesis of NFs a delicate process [32–34]. Therefore, in this work our focal point is to fabricate electrospun nanofiber with inherent luminescence property which could be potentially used as smart material for flexible display applications.

Rare earth ion doped metal oxides have been largely traversed for luminescent property. Alkaline earth metal yttrates (MY_2O_4, M = Sr, Ba, Ca) doped with rare earth ions have been known to showcase eminent optical emission. $SrY_2O_4:RE^{3+}$ (RE = Eu, Dy, Ce, Tb, Er, Gd, Sm, Nd) have been reported to be synthesized by solid state reaction method, solution combustion method, sol gel method, citrate sol gel method, polyol method, oil emulsion method, aldo-keto gel method and co-precipitation method [35]. Europium is one of the interesting and

* Corresponding author.
E-mail address: sbkondawar@yahoo.co.in (S.B. Kondawar).

https://doi.org/10.1016/j.mtcomm.2022.104950
Received 22 October 2022; Received in revised form 29 October 2022; Accepted 14 November 2022

Table 1
Stoichiometric ratio of precursors for synthesis of SrY_2O_4 host and Eu^{3+} doped SrY_2O_4 NFs.

Sample	Polyvinyl-pyrrolidone (PVP) (12 wt %)	Dimethyl-formamide (DMF)	Strontium nitrate (40 mmol)	Yttrium nitrate (80 mmol)	Europium nitrate
SrY_2O_4 host NFs	1.2 g	10 mL	0.084 g	0.308 g	–
SrY_2O_4: Eu(2)	1.2 g	10 mL	0.084 g	0.308 g	0.010 g (2 mol %)
SrY_2O_4: Eu(6)	1.2 g	10 mL	0.084 g	0.308 g	0.031 g (6 mol %)
SrY_2O_4: Eu (10)	1.2 g	10 mL	0.084 g	0.308 g	0.051 g (10 mol %)
SrY_2O_4: Eu (14)	1.2 g	10 mL	0.084 g	0.308 g	0.072 g (14 mol %)

versatile lanthanides that has been widely explored for luminescence applications because of red optical emission. SrY_2O_4:Eu^{3+} (SYO:Eu) has $CaFe_2O_4$ like structure and manifests sublime down conversion luminescence property. The long-lived transition $^5D_0 \rightarrow {}^7F_2$ of Eu^{3+} produces highly intense emission line at 612 nm. The near ultraviolet (NUV) excitation of 395 nm facilitates the use of europium ions in light emitting phosphors and other display applications [36–48].

To the best of our knowledge, SrY_2O_4 (SYO) has not yet been synthesized in nanofiber form. Here in the present work, we report the facile fabrication of novel Eu^{3+} ion doped SYO electrospun NFs which can be used to enhance the aesthetic performance of the smart materials to be used for flexible display applications. Upon NUV excitation, SYO:Eu NFs showcase red light emission. The diameter of the NFs has been efficaciously controlled in the electrospinning process. The effect of temperature and Eu^{3+} dopant concentration on SYO NFs have been examined systematically. The spectroscopic characterization, morphological, thermal, and optical analysis of SYO:Eu NFs have been studied using FTIR, SEM, HRTEM-SAED, TGA/DSC and PL.

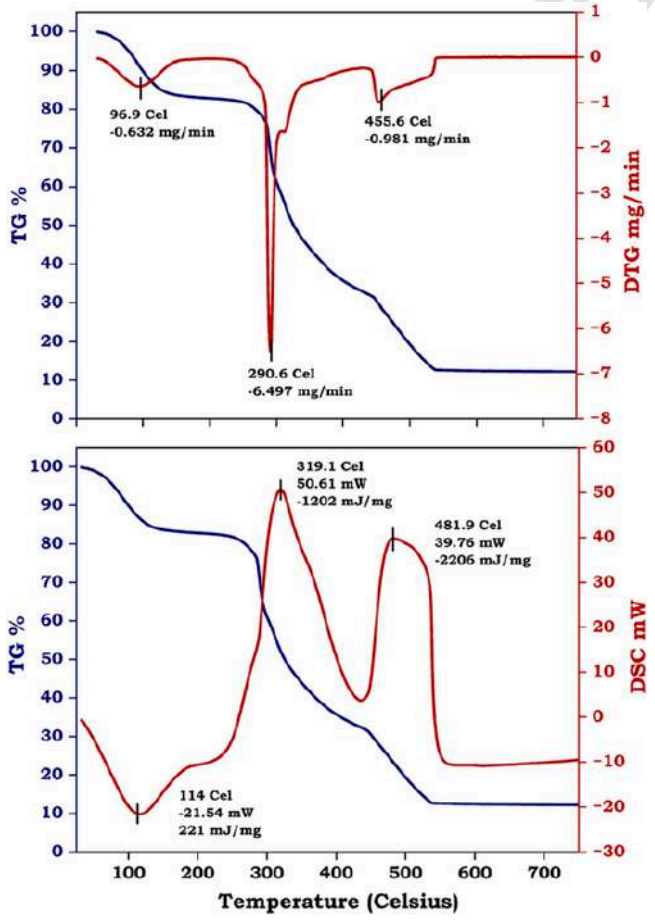

Fig. 1. TGA/DTG/DSC thermograms of SYO:Eu(10) NFs.

2. Experimental techniques

Polyvinylpyrrolidone (PVP, M_w 13,00,000, Sigma Aldrich) was utilised as a backbone for obtaining the one-dimensional NF structure. Strontium nitrate ($Sr(NO_3)_2$, Himedia), Yttrium nitrate hexahydrate ($Y(NO_3)_2.6H_2O$, Himedia) and Europium nitrate pentahydrate ($Eu(NO_3)_3.5H_2O$, Sigma Aldrich) were used as metal precursors.

The stoichiometric amount of solvent and metal precursors used in the synthesis of SYO host and Eu^{3+} ion doped SYO NFs is presented in Table 1. The resultant solution was magnetically stirred overnight to obtain a homogeneous polymer-salt precursor solution. The viscosity of the final spinnable solution for preparation of SrY_2O_4 host NFs was calculated using LABMAN Digital Rotational Viscometer LMDV-60 and the viscosity was obtained to be 154 cP. Electrospinning method was chosen for synthesis of SYO NFs using ESPIN-NANO instrument. The viscous precursor solution was loaded in a 10 mL plastic syringe with a metallic nozzle. The nozzle of the syringe was connected to high voltage power supply of 25 kV. The flow rate of the precursor solution was set to 0.7 mLh^{-1}. The collector was placed at 16 cm from the tip of the syringe nozzle. The as-spun SYO/PVP NFs were collected on an aluminium foil covered onto a grounded steel electrode plate and dried overnight at 70 °C in a vacuum oven. The pure phase of host SYO NFs was obtained by calcination of the as-spun NFs at 900 °C under a constant heating rate of 1 °C min^{-1} for 2 h in muffle furnace. For the preparation of SYO:Eu NFs, the concentration of europium dopant was varied from 2 mol % to 14 mol %, while all the other measurements were kept same. The effect of Eu^{3+} ions on SYO NFs have been examined in the present work as SYO:Eu(2), SYO:Eu(6), SYO:Eu(10), and SYO:Eu(14) for 2 mol %, 6 mol %, 10 mol % and 14 mol % Eu^{3+} ion doped SYO NFs, respectively.

The thermogravimetric analysis of SYO:Eu NFs was performed on Hitachi-STA7300 TGA/DSC analyser under nitrogen atmosphere. The thermogram was recorded from room temperature up to 750 ^{0}C. Scanning electron microscopy (SEM) images were recorded using ZEISS-EVO-18. Firstly, the NFs were DC sputtered with gold-palladium under 15 mA current. The SEM images were captured by electron gun composed of tungsten filament at an accelerating voltage of 5 kV. High resolution transmission electron microscopy (HR-TEM) and selected area electron diffraction (SAED) images were obtained using Jeol/JEM 2100 comprising of LaB_6 electron gun and operating at 200 kV. The instrument has point resolution of 0.23 nm and lattice resolution of 0.14 nm. The X-Ray diffraction studies were carried out on Bruker D8 Advance X-ray diffractometer at room temperature. The XRD spectra was recorded in the range of 2θ from 10^0 to 80^0 with 0.02^0 step size. The FTIR spectra was recorded on JASCO FTIR-4700 spectrometer in the form of % transmittance from 450 to 4000 cm^{-1} with a resolution of 4 cm^{-1}. The PL study was carried out with the help of Shimadzu RF-5301PC Spectrofluorometer with 150 W Xenon lamp as light source and the spectra was obtained in the wavelength range of 220 – 750 nm having S/N ratio of 150.

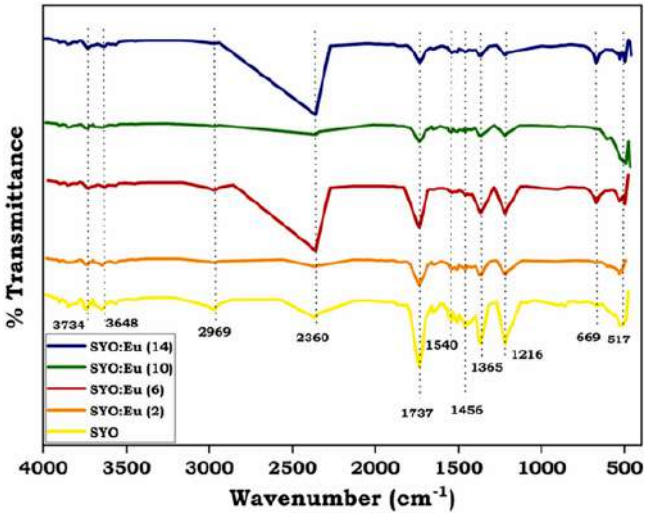

Fig. 2. Effect of Eu^{3+} concentration on FTIR spectra of SYO NFs.

3. Results and discussion

3.1. Thermal analysis

To investigate the thermal decomposition pattern and subsequently decide suitable temperature for effective calcination of the SYO:Eu NFs, thermogravimetric analysis was carried out. Moreover, the SYO:Eu(10) NFs were chosen as representative material for the thermal analysis since the PL study shows the highest emission intensity for 10 mol % Eu^{3+} concentration. The TGA and DSC thermograms of SYO:Eu(10) NFs were recorded at 20 °C heating rate from ambient temperature to 750 °C under nitrogen atmosphere.

The perusal of thermogram of SYO:Eu(10) NFs (Fig. 1) depicts the NFs undergo thermal decomposition in three substantial stages. The first stage of thermal decomposition occurred in temperature range 25–130 °C with 17 % weight loss and an endothermic peak in the DSC curve observed at 114 °C may be attributed to the loss of water molecules indicating the presence of trapped moisture in the NFs [49]. The second stage of decomposition observed in temperature range 130–440 °C showed 51 % mass loss with an exothermic peak at 319 °C. Furthermore, the third stage of decomposition indicated 19 % mass loss in temperature range 440–550 °C with an exothermic peak at 481.9 °C [50,51]. The comprehensive study of TGA and DSC thermograms as well as the exothermic peaks observed for second and third stages of decomposition suggest that the SYO:Eu(10) NFs undergo steady mass loss up to 550 °C due to the gradual breakdown of PVP polymeric chain and loss of organic moiety. However, there was no further change in weight loss above 550 °C and the % residue remained constant suggesting the formation of stable inorganic phase [40]. Moreover, the half decomposition temperature (T_h) of the SYO:Eu(10) as-spun NFs was found to be 330 °C suggesting higher thermal stability of the NFs. Therefore, based on thermogravimetric analysis data, all the synthesized materials have been calcined above 550 °C, viz. 600, 700, 800, and 900 °C for 2 h under a constant heating rate of 1 °C min^{-1} for efficient calcination and further studies.

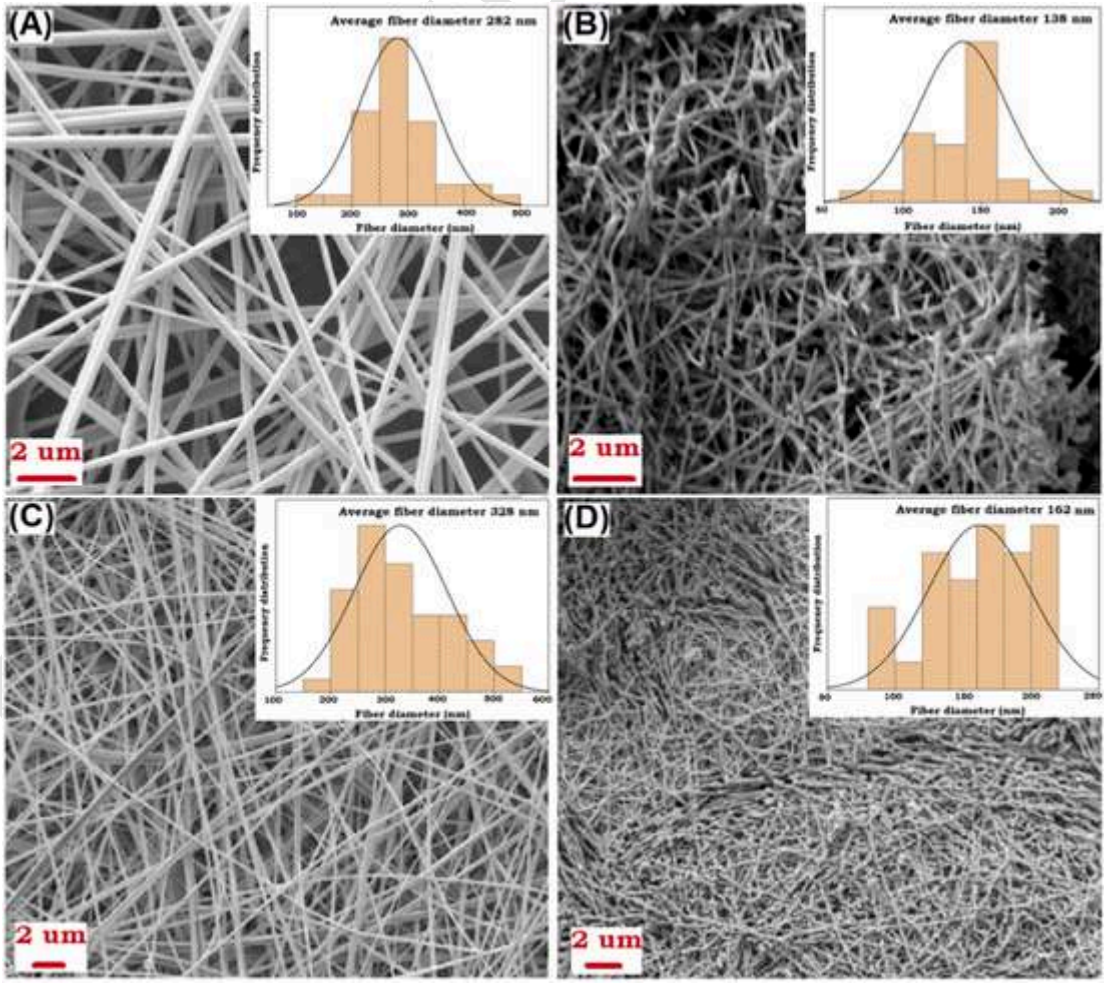

Fig. 3. SEM image and histogram of (A) SYO/PVP NFs, (B) Calcined SYO NFs, (C) SYO:Eu(10)/PVP NFs and (D) Calcined SYO:Eu(10) NFs.

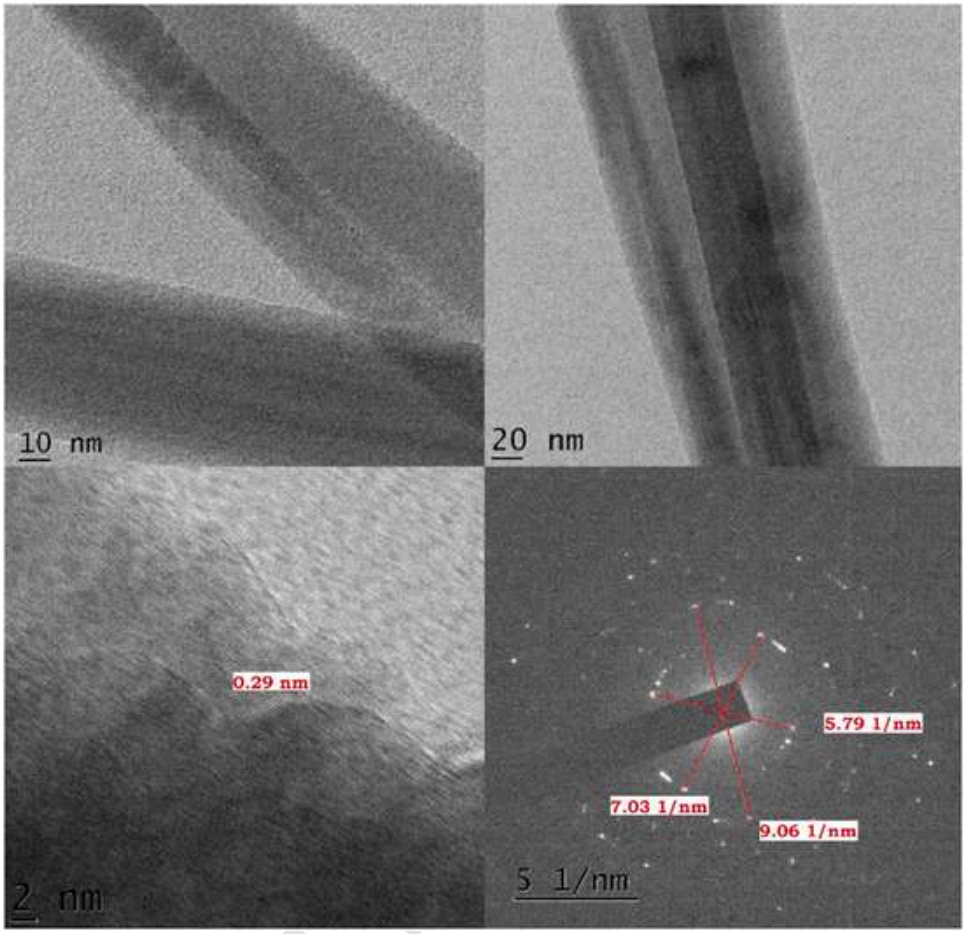

Fig. 4. HR-TEM images and SAED pattern for SYO NFs.

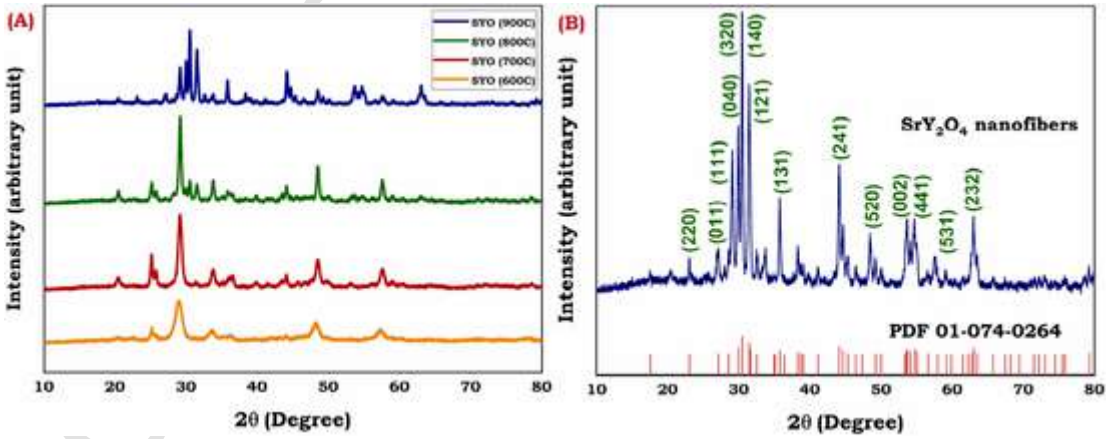

Fig. 5. (A) Effect of temperature on XRD of SYO NFs, (B) XRD spectra of SYO NFs calcined at 900 °C.

3.2. Fourier transform infrared spectroscopy (FTIR)

Fig. 2 presents the relative FTIR spectra of SYO NFs and SYO:Eu NFs prepared by doping with varying concentrations of Eu^{3+}. The FTIR spectrum of SYO NFs shows a peak at 2969 cm^{-1} due to asymmetric C–H stretching vibrations whereas the sharp peak observed at 1365 cm^{-1} relate to C-H bending vibrations. The strong and intense peak observed at 1737 cm^{-1} arises due to ν(C═O) stretching vibrations of the carbonyl group [52]. The disappearance of characteristic peaks of PVP on calcination suggest the gradual breakdown of PVP chain and loss of organic moiety post calcination which is also supported by the TGA and DSC studies. The peaks appearing in the range of 1200–1600 cm^{-1} are due to Sr–O vibrations. The peaks appearing in the range 3648–3734 cm^{-1} are assigned to O-H vibrations of water molecules indicating the presence of trapped moisture [51]. The sharp peak observed at 517 cm^{-1} is assigned to Y-O vibration, whereas the medium peak is observed at 669 cm^{-1} is due to O-Y-O bond deformation because of enlargement in the lattice of SYO after calcination [40,53]. The peak positions in all the spectra remain almost same and the corresponding peak values do not shift with increase in the Eu^{3+} concentration in the NFs which implies the greater stability of the structure [36].

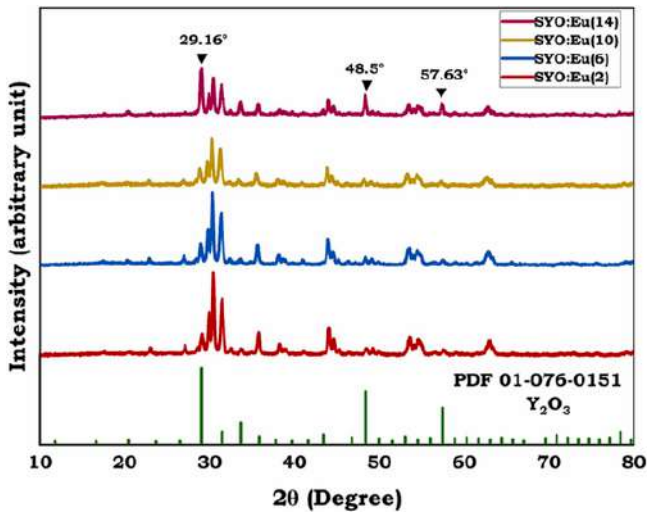

Fig. 6. Effect of Eu^{3+} concentration on SYO NFs.

3.3. Scanning electron microscopy (SEM)

Fig. 3 shows the SEM image and histogram of SYO NFs and SYO:Eu (10) NFs before and after calcination at 900 °C. It can be clearly seen that the SYO NFs appear to be continuous, smooth, and uniform before calcination with an average diameter of 282 nm. However, post calcination the SYO NFs shrink to a diameter of 138 nm. The NFs appear slightly broken because the spine of NFs is lost with the loss of PVP polymer and remaining residue during heat treatment. The SYO:Eu (10) NFs have an average diameter of 328 nm prior calcination and 162 nm post calcination, respectively. The comparative increase in the diameter of SYO:Eu(10) NFs can be attributed to the incorporation of dopant as depicted in Table 1 [54]. For doping SrY_2O_4 host NFs, additional amount of europium nitrate is added to the SrY_2O_4 host precursor solution.The comparative increase in diameter is observed in both as-spun and calcined Eu doped SrY_2O_4 NFs. It can notably be seen that the fiber structure is very well maintained for both the materials irrespective of the heat treatment. As compared to bulk counterparts, NFs have the advantage of high surface area to volume ratio and reduced internal scattering which enhances their luminescence property. Therefore, the synthesized NFs can be utilised for flexible display applications.

3.4. High resolution transmission electron microscopy (HR-TEM)

Observation of SYO NFs under HR-TEM (Fig. 4) revealed that the SYO NFs remain uniform and smooth post calcination and confirm the average diameter of 135 nm as visualized in the SEM analysis. The interplanar spacing of 0.29 nm depicted in the HR-TEM image corresponds to (320) plane which is also the most intense and abundant according to the ICDD powder diffraction file (PDF) no. 01–074–0264. The other significant planes identified from the SAED image include (011), (121) and (140) planes which very well agrees with the XRD data. The SAED pattern confirms the polycrystalline nature of SYO NFs.

3.5. X-Ray diffraction (XRD)

Fig. 5(A) shows the XRD profiles of SYO NFs calcined at different temperatures. The XRD spectra of SYO NFs treated at 600 °C comprises of peaks attributing to Y_2O_3 which shows that the temperature was not

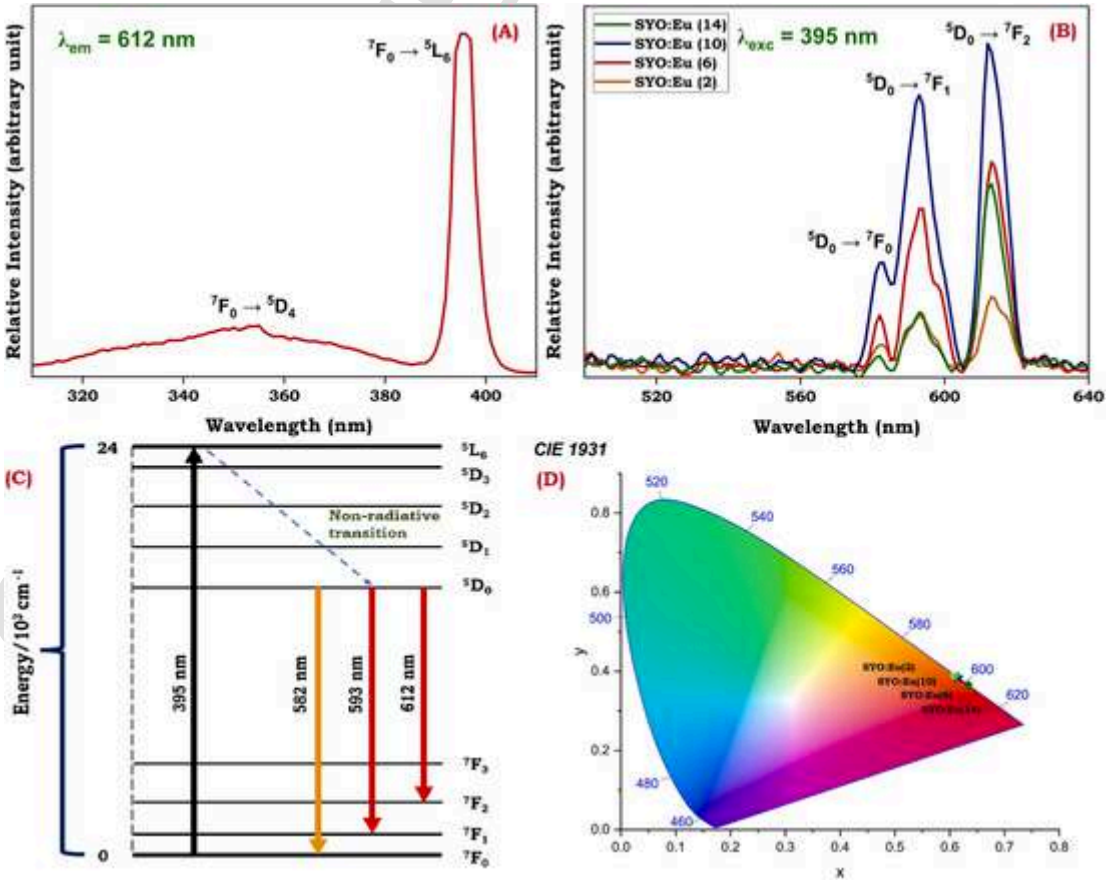

Fig. 7. (A) PL excitation spectrum for SYO:Eu NFs monitored at 612 nm, (B) PL emission spectra for SYO:Eu NFs under 395 nm excitation, (C) Energy level diagram for different transitions in SYO:Eu NFs, and (D) CIE plot for SYO:Eu NFs with different concentration.

Table 2
Colour purity of Eu^{3+} doped SYO NFs calculated using CIE x and y coordinates.

SYO:Eu Nanofibers	CIE (x, y)	White light (x_i, y_i)	Dominant wavelength (x_d, y_d)	Colour purity (%)
SYO:Eu (2)	(0.608, 0.390)	(0.333. 0.333)	(0.676, 0.323)	88.26
SYO:Eu (6)	(0.615, 0.383)	(0.333. 0.333)	(0.676, 0.323)	83.45
SYO:Eu (10)	(0.612, 0.387)	(0.333. 0.333)	(0.676, 0.323)	83.28
SYO:Eu (14)	(0.633, 0.365)	(0.333. 0.333)	(0.676, 0.323)	87.95

adequate for complete degradation of $Sr((NO)_3)_2$ [53]. However, with the consequent increase in temperature viz. 700, 800, and 900 °C, the peaks realign, and phase purity of SYO NFs is greatly improved. The XRD profile of SYO NFs calcined at 900 °C is found to be in complete agreement with ICDD PDF no. 01–074–0264 for SYO (Fig. 5(B)) [55]. The SYO NFs belong to orthorhombic crystal system with *Pnam* (62) space group [36]. The lattice constants of SYO NFs are $a = 10.08\ A^0$, $b = 11.91\ A^0$, $c = 3.4\ A^0$ [56]. The intensities of the diffraction peaks increase with the temperature which indicates that purity and crystallinity of SYO NFs is greatly enhanced, and the optimum results are obtained at 900 °C. The semi-quantitative analysis of SYO NFs calcined at 900 °C showcase a phase purity of 62.7 % for SrY_2O_4, 23.7 % for α-Sr and 13.6 % for Y_2O_3. XRD profile of SYO NFs illustrate significantly intense peaks at 30.524^0, 31.549^0, 35.868^0, 44.212^0, 53.580^0, 53.888^0, 54.788^0, 55.118^0, 63.206^0, and 62.902^0 which correspond to miller indices planes of (320), (121), (131), (331) and (241), (360), (002), (441), (521) and (610), (042), (322), respectively.

Effect of Eu^{3+} ion concentration on XRD profiles of SYO NFs is depicted in the Fig. 6. The change in the diffraction peak intensities indicate that the dopant has been efficiently housed into the host SYO NFs. The ionic radius of dopant has a significant role for incorporation into the host matrix. The Sr^{2+}, Y^{3+} and Eu^{3+} ions have ionic radii of ($1.13\ A^0$), ($0.89\ A^0$) and ($0.95\ A^0$) respectively [35,56]. Due to comparable ionic size and charge compensation, Y^{3+} ions in host lattice are replaced by Eu^{3+} ions which is very clearly observed in the XRD spectra. The peak intensity at $2\theta = 29.160°$, 48.5° and 57.63° corresponds to Y_2O_3 (ICDD PDF no. 01–076–0151) which increases with dopant concentration. This intensity is maximum for SYO:Eu(14) NFs, since more dopant is added and all the Eu^{3+} ions are incorporated into the host lattice, which confirms that due to same charge and equivalent ionic radius, Y^{3+} ions are substituted by Eu^{3+} ions on doping.

3.6. Photoluminescence (PL)

The host SYO NFs do not possess significant luminescence property, however on doping with Eu^{3+} ions, it showed remarkable emission spectra [35]. Fig. 7(A) represents the PL excitation spectra for Eu^{3+} doped SYO NFs. The excitation spectrum was observed under 612 nm emission wavelength. It comprises of a broad band at 356 nm and a sharp peak at 395 nm which can be assigned to the transitions from $^7F_0 \rightarrow {}^5D_4$ and $^7F_0 \rightarrow {}^5L_6$ levels respectively [57–59]. PL emission spectra of SYO NFs monitored at 395 nm illustrates the characteristic emission of Eu^{3+} at 582 nm, 593 nm, and 612 nm Fig. 7(B). The transitions between $^5D_0 \rightarrow {}^7F_J$ ($J = 0, 1, 2$) are responsible for Eu^{3+} emission spectra [60]. Fig. 7(C) displays the energy level diagram for different transitions in SYO:Eu NFs. The strongest emission band appears at 612 nm which correspond to electric dipole transition $^5D_0 \rightarrow {}^7F_2$ resulting from lack of inversion symmetry [35–37]. The bands located at 582 nm and 593 nm originate from magnetic dipole transition $^5D_0 \rightarrow {}^7F_0$ and $^5D_0 \rightarrow {}^7F_1$ [60]. The appearance of $^5D_0 \rightarrow {}^7F_1$ transition confirm that Eu^{3+} ions have been substituted at Y^{3+} sites owing to comparable ionic radii [61]. The emission spectra of SYO:Eu NFs showcase slight splitting of $^5D_0 \rightarrow {}^7F_1$ and $^5D_0 \rightarrow {}^7F_2$ transition lines which clearly shows that the coordination environment, crystal structure and the host composition has significant effect on luminescence properties [62]. The effect of dopant concentration on the emission intensity can be invariably seen in Fig. 7(B). As the concentration of Eu^{3+} ion is increased from 2 mol % to 10 mol %, the intensity goes on increasing. However, the intensity decreases significantly for 14 mol % due to concentration quenching phenomenon. Quenching occurs because Eu^{3+} ions become much closely spaced and their mutual interaction results in charge transfer, thereby resulting in minimised intensity. The optimised maximum emission intensity was obtained for SYO NFs doped with 10 mol % Eu^{3+} ions, henceforth it can be used for varied light emitting applications.

The luminescent colours for SYO:Eu NFs were identified from Commission Internationale de l'Eclairage (CIE) coordinates. Fig. 7(D) shows the CIE 1931 plot for different Eu^{3+} ion concentrations. The doping concentration does not have any significant effect on CIE coordinates and the SYO:Eu NFs emit red colour. The colour purity of SYO:Eu NFs was calculated using the formula [63];

$$Colour\ \ purity = \frac{\sqrt{(x-x_i)^2+(y-y_i)^2}}{\sqrt{(x_d-x_i)^2+(y_d-y_i)^2}} \times 100\%$$

The SYO NFs doped with 2 mol % Eu^{3+} ions have maximum colour purity of 88.26 % (Table 2). From good colour purity, SYO:Eu NFs can be potential candidates for optical devices and display applications.

4. Conclusion

Novel SYO:Eu NFs have been successfully synthesized for the first time using electrospinning. SYO:Eu NFs were studied at different calcination temperatures. SEM analysis of SYO:Eu NFs revealed shrinkage of NFs post calcination at 900 °C with consequent decrease in average diameter from 328 nm to 162 nm. The XRD profile confirmed that SYO NFs belong to orthorhombic crystal system with *Pnam* space group. The significant effect of ionic radii and charge compensation on XRD spectra have been clearly observed with substitution of Y^{3+} ions by Eu^{3+} ions. SYO:Eu NFs exhibited remarkable emission in red region upon NUV excitation. The emission spectra are comprised of the characteristic $^5D_0 \rightarrow {}^7F_2$ transition emission of Eu^{3+} ion at 612 nm along with additional peaks at 582 nm and 593 nm. Optimum emission intensity have been recorded for SYO:Eu(10) NFs while concentration quenching was observed for SYO:Eu(14) NFs. SYO:Eu NFs can potentially be used for flexible devices and smart display applications owing to its flexibility and inherent luminescence property.

CRediT authorship contribution statement

Mahelaqua A. Haque : Conceptualization, Methodology, Writing – original draft. **Mahejabeen Azizul Haque :** Resources, Visualization. **Subhash B. Kondawar :** Supervision, Project administration, Resources, Writing – review & editing.

Declaration of Competing Interest

The authors declare that they have no known competing financial interests or personal relationships that could have appeared to influence the work reported in this paper.

Data Availability

Data will be made available on request.

Acknowledgements

The authors are thankful to DST-SAIF Cochin, India for providing TGA, DSC, XRD, and HRTEM-SAED results. The authors also acknowledge Bajaj College of Science, Wardha for XRD spectral analysis. The authors are grateful to Department of Physics, Rashtrasant Tukadoji Maharaj Nagpur University, Nagpur, for providing SEM and FTIR results.

References

[1] D.C. Celikel, Smart E-Textile Materials, in: N. Tasaltin, P.S. Nnamchi, S. Saud (Eds.), Advanced functional materials [Internet], IntechOpen, London, 2020, pp. 1–16, https://doi.org/10.5772/intechopen.92439.

[2] L. Liu, W. Xu, Y. Ding, S. Agarwal, A. Greiner, G. Duan, A review of smart electrospun fibers toward textiles, Comp. Commun. 22 (2020) 100506, https://doi.org/10.1016/j.coco.2020.100506.

[3] M. Ghahremani Honarvar, M. Latifi, Overview of wearable electronics and smart textiles, J. Text. Inst. 108 (4) (2017) 631–652, https://doi.org/10.1080/00405000.2016.1177870.

[4] M. Chen, Y. Ma, J. Song, C.F. Lai, B. Hu, Smart clothing: connecting human with clouds and big data for sustainable health monitoring, Mob. Net. Appl. 21 (5) (2016) 825–845, https://doi.org/10.1007/s11036-016-0745-1.

[5] A. Bratovcic, Different applications of nanomaterials and their impact on the environment, Int. J. Mater. Sci. Eng. 5 (1) (2019) 1–7, https://doi.org/10.14445/23948884/IJMSE-V5I1P101.

[6] P. Kumar, S. Singh, B.K. Gupta, Future prospects of luminescent nanomaterial based security inks: from synthesis to anti-counterfeiting applications, Nanoscale 8 (30) (2016) 14297–14340, https://doi.org/10.1039/C5NR06965C.

[7] J. Yu, M. Luo, Z. Lv, S. Huang, H.H. Hsu, C.C. Kuo, Y. Zhou, Recent advances in optical and optoelectronic data storage based on luminescent nanomaterials, Nanoscale 12 (46) (2020) 23391–23423, https://doi.org/10.1039/D0NR06719A.

[8] S. Kwon, Y.H. Hwang, M. Nam, H. Chae, H.S. Lee, Y. Jeon, K.C. Choi, Recent progress of fiber shaped lighting devices for smart display applications—a fibertronic perspective, Adv. Mater. 32 (5) (2020) 1903488, https://doi.org/10.1002/adma.201903488.

[9] M. Cinquino, C.T. Prontera, M. Pugliese, R. Giannuzzi, D. Taurino, G. Gigli, V. Maiorano, Light-emitting textiles: device architectures, working principles, and applications, Micromachines 12 (6) (2021) 652, https://doi.org/10.3390/mi12060652.

[10] X. Shi, Y. Zuo, P. Zhai, J. Shen, Y. Yang, Z. Gao, H. Peng, Large-area display textiles integrated with functional systems, Nature 591 (7849) (2021) 240–245, https://doi.org/10.1038/s41586-021-03295-8.

[11] M. Haque, Nano fabrics in the 21st century: a review, Asian J. Nanosci. Mater. 2 (2) (2019) 131–148, https://doi.org/10.26655/ajnanomat.2019.3.2.

[12] Z. Gong, Z. Xiang, X. OuYang, J. Zhang, N. Lau, J. Zhou, C.C. Chan, Wearable fiber optic technology based on smart textile: a review, Materials 12 (20) (2019) 3311, https://doi.org/10.3390/ma12203311.

[13] C.W. Kan, Y.L. Lam, Future trend in wearable electronics in the textile industry, Appl. Sci. 11 (9) (2021) 3914, https://doi.org/10.3390/app11093914.

[14] A. Angelucci, M. Cavicchioli, I.A. Cintorrino, G. Lauricella, C. Rossi, S. Strati, A. Aliverti, Smart textiles and sensorized garments for physiological monitoring: a review of available solutions and techniques, Sensors 21 (3) (2021) 814, https://doi.org/10.3390/s21030814.

[15] X. Hu, Y. Dou, J. Li, Z. Liu, Buckled structures: fabrication and applications in wearable electronics, Small 15 (32) (2019) 1804805, https://doi.org/10.1002/smll.201804805.

[16] Q. Zhang, Y.L. Wang, Y. Xia, P.F. Zhang, T.V. Kirk, X.D. Chen, X. D, Textile-only capacitive sensors for facile fabric integration without compromise of wearability, Adv. Mater. Tech. 4 (10) (2019) 1900485, https://doi.org/10.1002/admt.201900485.

[17] A.A. Simegnaw, B. Malengier, G. Rotich, M.G. Tadesse, L. Van Langenhove, Review on the integration of microelectronics for E-Textile, Materials 14 (17) (2021) 5113, https://doi.org/10.3390/ma14175113.

[18] E.A. Hassan, M.A. Ahmed, S. Zhu, O.K. Alebeid, Fibre-based wearable electronic technology for personal protective clothing, in: Protective textiles from natural resources, Woodhead Publishing, 2022, pp. 511–547, https://doi.org/10.1016/B978-0-323-90477-3.00019-5.

[19] A.A. Basheer, Advances in the smart materials applications in the aerospace industries, Aircr. Eng. Aerosp. Tech. 92 (7) (2020) 1027–1035, https://doi.org/10.1108/AEAT-02-2020-0040.

[20] A. Raza, U. Hayat, T. Rasheed, M. Bilal, H.M. Iqbal, "Smart" materials-based near-infrared light-responsive drug delivery systems for cancer treatment: a review, J. Mater. Res. Tech. 8 (1) (2019) 1497–1509, https://doi.org/10.1016/j.jmrt.2018.03.007.

[21] C. Mendes-Felipe, J. Oliveira, I. Etxebarria, J.L. Vilas-Vilela, S. Lanceros-Mendez, State-of-the-art and future challenges of UV curable polymer-based smart materials for printing technologies, Adv. Mater. Tech. 4 (3) (2019) 1800618, https://doi.org/10.1002/admt.201800618.

[22] Z. Li, F. Yang, Y. Yin, Smart materials by nanoscale magnetic assembly, Adv. Func. Mater. 30 (2) (2020) 1903467, https://doi.org/10.1002/adfm.201903467.

[23] P. Karami, B. Khorshidi, M. McGregor, J.T. Peichel, J.B. Soares, M. Sadrzadeh, Thermally stable thin film composite polymeric membranes for water treatment: a review, J. Clean. Prod. 250 (2020) 119447, https://doi.org/10.1016/j.jclepro.2019.119447.

[24] H. Han, J. Park, S.Y. Nam, K.J. Kim, G.M. Choi, S.S. Parkin, J.T. Irvine, Lattice strain-enhanced exsolution of nanoparticles in thin films, Nat. Commun. 10 (1) (2019) 1–8, https://doi.org/10.1038/s41467-019-09395-4.

[25] N.K. Jangid, S. Jadoun, N. Kaur, A review on high-throughput synthesis, deposition of thin films and properties of polyaniline, Eur. Polym. J. 125 (2020) 109485, https://doi.org/10.1016/j.eurpolymj.2020.109485.

[26] R. Shwetharani, H.R. Chandan, M. Sakar, G.R. Balakrishna, K.R. Reddy, A.V. Raghu, Photocatalytic semiconductor thin films for hydrogen production and environmental applications, Int. J. Hydrog. Energy 45 (36) (2020) 18289–18308, https://doi.org/10.1016/j.ijhydene.2019.03.149.

[27] H. Lin, C. Rosu, L. Jiang, V.A. Sundar, V. Breedveld, D.W. Hess, Nonfluorinated superhydrophobic chemical coatings on polyester fabric prepared with kinetically controlled hydrolyzed methyltrimethoxysilane, Ind. Eng. Chem. Res. 58 (33) (2019) 15368–15378, https://doi.org/10.1021/acs.iecr.9b02471.

[28] D. Patch, I. Koch, D. Peloquin, D. O'Carroll, K. Weber, Development and validation of a method for the weathering and detachment of representative nanomaterials from conventional silver-containing textiles, Chemo 284 (2021) 131269, https://doi.org/10.1016/j.chemosphere.2021.131269.

[29] T.M. Akshat, S. Misra, M.Y. Gudiyawar, J. Salacova, M. Petru, Effect of electrospun nanofiber deposition on thermo-physiology of functional clothing, Fibers Polym. 20 (5) (2019) 991–1002, https://doi.org/10.1007/s12221-019-9100-z.

[30] A.C. Silva, A.J. Silvestre, C.S. Freire, C. Vilela, Modification of textiles for functional applications, in: Fundamentals of natural fibres and textiles, Woodhead Publishing, 2021, pp. 303–365, https://doi.org/10.1016/B978-0-12-821483-1.00010-3.

[31] Y. Zhao, X. Li, J. Shen, C. Gao, B. Van der Bruggen, The potential of Kevlar aramid nanofiber composite membranes, J. Mater. Chem. A 8 (16) (2020) 7548–7568, https://doi.org/10.1039/D0TA01654C.

[32] G. Sharma, S. Rastogi, B. Kandasubramanian, Smart electrospun materials, Electro Mater. Allied Appl. (2020) 351–378, https://doi.org/10.1002/9781119655039.ch12.

[33] S.B. Kondawar, C.N. Pangul, M.A. Haque, Polymer Nanofibers via Electrospinning for Flexible Devices, in: S.K. Tiwari, K. Sharma, V. Sharma, V. Kumar (Eds.), Electrospun Nanofibers. Springer Series on Polymer and Composite Materials, Springer, Cham, 2021, pp. 53–86, https://doi.org/10.1007/978-3-030-79979-3_3.

[34] S.B. Kondawar, M.A. Haque, C.N. Pangul, Application of Electrospun Materials in LEDs, Polym. Light. Devices Disp. (2020) 99–123, https://doi.org/10.1002/9781119654643.ch5.

[35] R. Priya, S. Kaur, U. Sharma, O.P. Pandey, S.J. Dhoble, A review on recent progress in rare earth and transition metals activated SrY_2O_4 phosphors, J. Mater. Sci.: Mater. Elec 31 (16) (2020) 13011–13027, https://doi.org/10.1007/s10854-020-03930-6.

[36] S.P. Ghorpade, R.H. Krishna, R.M. Melavanki, V. Dubey, N.R. Patil, Effect of Eu^{3+} on optical and energy bandgap of SrY_2O_4 nanophosphors for FED applications, Optik 208 (2020) 164533, https://doi.org/10.1016/j.ijleo.2020.164533.

[37] D.R. Taikar, Synthesis and luminescence property of SrY_2O_4: M (M = Eu^{3+} Tb^{3+},Sm^{3+} Tb3+,Sm3+, Ce3+, Bi3+) phosphors, J. Lumin. 204 (2018) 24–29, https://doi.org/10.1016/j.jlumin.2018.07.040.

[38] E. Pavitra, G.S.R. Raju, W. Park, J.S. Yu, Concentration and penetration depth dependent tunable emissions from Eu^{3+} co-doped SrY_2O_4:Dy^{3+} nanocrystalline phosphor, New J. Chem. 38 (1) (2014) 163–169, https://doi.org/10.1039/C3NJ00987D.

[39] R.K. Tamrakar, K. Upadhyay, Combustion synthesis and luminescence behaviour of the Tb^{3+} doped SrY_2O_4 phosphor, J. Elect. Mater. 47 (1) (2018) 651–654, https://doi.org/10.1007/s11664-017-5825-x.

[40] S.P. Ghorpade, N. Kottam, R. Melavanki, N.R. Patil, Photoluminescence, TGA/DSC and photocatalytic activity studies of Dy^{3+} doped SrY_2O_4 nanophosphors, RSC Adv. 10 (36) (2020) 21049–21056, https://doi.org/10.1039/D0RA03094E.

[41] V. Singh, K. Swapna, S. Kaur, A.S. Rao, J.L. Rao, Narrow-band UVB-emitting Gd-doped SrY_2O_4 phosphors, J. Elecron. Mater. 49 (5) (2020) 3025–3030, https://doi.org/10.1007/s11664-020-08032-x.

[42] R. Wei, Z. Zheng, Y. Shi, X. Peng, H. Wang, X. Tian, H. Guo, Tunable emission with excellent thermal stability in single-phased SrY_2O_4: Bi^{3+}, Eu^{3+} phosphors for UV-LEDs, J. Alloy. Comp. 767 (2018) 403–408, https://doi.org/10.1016/j.jallcom.2018.07.101.

[43] S. Bhatia, R. Priya, D. Kumar, S. Upadhyay, O.P. Pandey, Structural and luminescent studies of titanium co-doped SrY_2O_4: Eu phosphors, Lum (2022), https://doi.org/10.1002/bio.4335.

[44] I. Suryawanshi, R. Kalia, R.K. Kunchala, S.L. Mudavath, B.S. Naidu, Detection of latent fingerprints using luminescent $Gd_{0.95}Eu_{0.05}PO_4$ nanorods, J. Rare Earths. 40 (4) (2022) 572–578, https://doi.org/10.1016/j.jre.2021.01.015.

[45] S.P. Singh, S. Srinidhi, R.K. Kunchala, R. Kalia, S.N. Achary, B.S. Naidu, Structural and excitation-dependent photoluminescence properties of $Bi_{0.95x}Gd_xEu_{0.05}PO_4(0\leq x\leq 0.95)$ solid solutions and their anticounterfeiting applications, Cryst. Growth Des. 21 (8) (2021) 4619–4631, https://doi.org/10.1021/acs.cgd.1c00467.

[46] I. Suryawanshi, S. Srinidhi, S. Singh, R. Kalia, R.K. Kunchala, S.L. Mudavath, B.S. Naidu, Downshifting and upconversion dual mode emission from lanthanide doped $GdPO_4$ nanorods for unclonable anti-counterfeiting, Mater. Today Comm. 26 (2021) 102144, https://doi.org/10.1016/j.mtcomm.2021.102144.

[47] I. Pushpendra, R.K. Kunchala, S.N. Achary, B.S. Naidu, $NaBi_{0.9}Eu_{0.1}(MoO_4)_2$

nanomaterials: tailoring the band gap and luminescence by La^{3+} substitution for light-emitting diodes, ACS Appl. Nano Mater. 2 (9) (2019) 5527–5537, https://doi.org/10.1021/acsanm.9b01111.

[48] I. Pushpendra, R.K. Kunchala, S.N. Achary, A.K. Tyagi, B.S. Naidu, Rapid, room temperature synthesis of Eu^{3+} Doped $NaBi(MoO_4)_2$ nanomaterials: structural, optical, and photoluminescence properties, Cryst. Growth Des. 19 (6) (2019) 3379–3388, https://doi.org/10.1021/acs.cgd.9b00267.

[49] D.Y. Lee, M.H. Lee, N.I. Cho, B.Y. Kim, Y.J. Oh, Effect of calcination temperature and atmosphere on crystal structure of $BaTiO_3$ nanofibers, Met. Mater. Int 16 (3) (2010) 453–457, https://doi.org/10.1007/s12540-010-0616-4.

[50] X. Li, M. Yu, Z. Hou, G. Li, W. Wang, Z. Cheng, J. Lin, One-dimensional $GdVO_4$: Ln^{3+} (Ln = Eu, Dy, Sm) nanofibers: electrospinning preparation and luminescence properties, J. Solid State Chem. 184 (1) (2011) 141–148, https://doi.org/10.1016/j.jssc.2010.11.019.

[51] F. Zhou, X. Zhao, H. Xu, C. Yuan, CeO_2 spherical crystallites: synthesis, formation mechanism, size control, and electrochemical property study, J. Phys. Chem. C. 111 (4) (2007) 1651–1657, https://doi.org/10.1021/jp0660435.

[52] S. Sundarrajan, A. Venkatesan, S.R. Agarwal, N.N.S.A. Ahamed, S. Ramakrishna, Fabrication of NiO/zirconium oxide nanofibers by electrospinning, Mater. Sci. Eng. C. 45 (2014) 369–373, https://doi.org/10.1016/j.msec.2014.09.029.

[53] S. Culas, A. Surendran, J. Samuel, Kinetic studies of the Non-Isothermal decomposition of strontium nitrate, Asian J. Chem. 25 (7) (2013) 3855, https://doi.org/10.14233/ajchem.2013.13820.

[54] T.E. Böncü, N. Ozdemir, Effects of drug concentration and PLGA addition on the properties of electrospun ampicillin trihydrate-loaded PLA nanofibers, Beilstein J. Nanotech. 13 (1) (2022) 245–254, https://doi.org/10.3762/bjnano.13.19.

[55] V. Dubey, J. Kaur, S. Agrawal, N.S. Suryanarayana, K.V.R. Murthy, Synthesis and characterization of Eu^{3+} doped SrY_2O_4 phosphor, Optik 124 (22) (2013) 5585–5587, https://doi.org/10.1016/j.ijleo.2013.03.153.

[56] R. Wei, J. Guo, K. Li, L. Yang, X. Tian, X. Li, H. Guo, Dual-emitting SrY_2O_4: Bi^{3+}, Eu^{3+} phosphor for ratiometric temperature sensing, J. Lumin. 216 (2019) 116737, https://doi.org/10.1016/j.jlumin.2019.116737.

[57] A. Ciric, L. Marciniak, M.D. Dramicanin, Self-referenced method for the Judd–Ofelt parametrisation of the Eu^{3+} excitation spectrum, Sci. Rep. 12 (1) (2022) 1–10, https://doi.org/10.1038/s41598-021-04651-4.

[58] S. Fazal, F. Zaman, S. Ali, Y. Iqbal, N. Chanithima, S. Tuscharoen, J. Kaewkhao, Investigation of europium-doped aluminium phosphate glass for red light generation, Ceram. Int. 48 (17) (2022) 24751–24757, https://doi.org/10.1016/j.scriptamat.2020.06.014.

[59] A. Hooda, S.P. Khatkar, A. Khatkar, R.K. Malik, S. Devi, J. Dalal, V.B. Taxak, Combustion synthesis, Judd–Ofelt parameters and optical properties of color tunable $Ba_3Y_4O_9$: Eu^{3+} nanophosphor for near-UV based WLEDs, J. Mater. Sci.: Mater. Electron. 30 (9) (2019) 8751–8762, https://doi.org/10.1007/s10854-019-01199-y.

[60] J. Chen, J. Wang, F. Zhang, D. Yan, G. Zhang, R. Zhuo, P. Yan, Structure and photoluminescence property of Eu-doped SnO_2 nanocrystalline powders fabricated by sol–gel calcination process, J. Phys. D. Appl. Phys. 41 (10) (2008) 105306, https://doi.org/10.1088/0022-3727/41/10/105306.

[61] V. Dubey, J. Kaur, S. Agrawal, Effect of europium doping levels on photoluminescence and thermoluminescence of strontium yttrium oxide phosphor, Mater. Sci. Sem. Proc. 31 (2015) 27–37, https://doi.org/10.1016/j.mssp.2014.10.052.

[62] H.J. Song, L.Q. Zhou, Y. Huang, L. Li, T. Wang, L. Yang, Synthesis, characterization and luminescent properties of $La_2Zr_2O_7$: Eu^{3+} nanorods, Chin. J. Chem. Phys. 26 (1) (2013) 83, https://doi.org/10.1063/1674-0068/26/01/83-87.

[63] D.R. Taikar, S. Tamboli, S.J. Dhoble, Synthesis and photoluminescence properties of Li_2SO_4: RE (RE = Eu^{3+}, Tb^{3+}, Gd^{3+} and Ce^{3+}) phosphors, Optik 139 (2017) 111–122, https://doi.org/10.1016/j.ijleo.2017.03.115.